Journal of Energy Storage 76 (2024) 109789

Contents lists available at ScienceDirect

Journal of Energy Storage

journal homepage: www.elsevier.com/locate/est

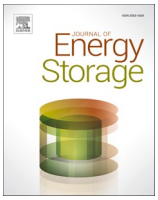

Research papers

Charge storage capacity of electromethanogenic biocathodes

D. Carrillo-Peña [a], G. Pelaz [a], R. Mateos [a], A. Escapa [a,b,*]

[a] Chemical and Environmental Bioprocess Engineering Group, Natural Resources Institute, Universidad de León, León 24071, Spain
[b] Department of Electrical Engineering and Automatic Systems, Universidad de León, León 24071, Spain

ARTICLE INFO

Keywords:
Biocathodes
Capacitance
Charge storage
Energy storage

ABSTRACT

Methanogenic biocathodes (MB) can convert CO_2 and electricity into methane. This feature, that allows them to potentially be used for long-term electrical energy storage, has aroused great interest during the past 10 years. MB can also operate as biological supercapacitors, a characteristic that can be exploited for short-term energy storage and that has received much less attention. In this study, we investigate the electrical charge storage capabilities of carbon-felt-based MB modified with graphene oxide. The charge-discharge experiments revealed that the potential of the electrode plays an important role during the discharging period: low potentials (−1.2 V vs Ag/AgCl) created an inrush of faradaic current that masked any capacitive current. At more positive potentials (−0.8 V vs Ag/AgCl), the biological electrodes were outperformed by the abiotic electrodes, and only when the potential was set at −1.0 V vs Ag/AgCl the graphene-modified biological electrode showed its superior charge storage capacity. Overall, results indicated that the graphene modification is crucial to obtain bioelectrodes with improved capacitance: untreated bioelectrodes showed a charge storage capacity inferior to that measured in the abiotic electrodes.

1. Introduction

In recent years, national and international institutions have set various targets for expanding the use of renewable energy, which has led to the installation of increasing amounts of renewable power across the globe. For example, in Spain, the share of renewables in power production has dramatically increased in the past 3 years, escalating from 38 % in 2018 to 47 % in 2021 [1]. However, the high penetration of renewable power sources —with their associated intermittent and inconsistent energy production profiles— usually results in surpluses of energy, that if not conveniently addressed can be lost (i.e.: curtailments) and/or cause severe stability issues to the grid [2]. It is thus expected that future power systems will need to implement large storage capacity to balance supply and demand on a real-time basis [3]. Currently, more than 90 % of the worldwide storage capacity corresponds to pumping hydropower [4]. Other less conventional technologies such as batteries or compressed air are moving towards commercial application, although they still require intensive research and ground-breaking developments to reduce costs and improve performance [5].

Bioelectrochemical systems (BES) can be seen as electrochemical devices in which at least one of the electrode reactions is biologically catalysed. In addition, and like any other electrochemical system, BES are reversible, which means that they can operate in galvanic mode and in electrolytic mode. The later allows BES to convert electrical energy into chemical energy, usually in the form of methane, hydrogen and/or other value-added products [6]. The process of converting electricity into methane in a BES is usually referred to as microbial electromethanogenesis (EM) [7]. By its very nature, EM can be classified among the Power-to-gas technologies, as it can potentially be used to store any surplus of renewable energy into methane [8]. In recent years, a growing number of studies exploring the potential of EM as an energy storage technology have been published, with emphasis on different aspects such as the influence of different operational parameters [9–11], reactor configuration [12], electrode materials [13,14] or the integration with renewable energies [15,16].

Another interesting feature of BES is that bioelectrodes can work as biological supercapacitors [17–19], thus enabling the storage of electrical energy on their surface. The inherent capacitive character of bioanodes have received significant attention since 2005, when Ieropoulos et al. [20] proved that they can store electrical charge when left in open circuit conditions. Later studies showed that fast redox reactions of the bacterial cytochromes present in electroactive biofilms makes them behave as pseudo-capacitors [21]. In Ter Heijne et al. [18], the authors proved that it is possible to measure separately the individual

* Corresponding author at: Department of Electrical Engineering and Automatic Systems, Universidad de León, León 24071, Spain.
E-mail address: adrian.escapa@unileon.es (A. Escapa).

https://doi.org/10.1016/j.est.2023.109789
Received 21 August 2023; Received in revised form 26 October 2023; Accepted 17 November 2023
Available online 22 November 2023

contribution of the electrode and the biofilm to the total bioelectrode (pseudo)-capacitance, reporting that the capacitance of the bioanode increased from 2 μF·cm^{-2} to 450 μF·cm^{-2} during biofilm growth. Deeke et al. [22] compared two plain graphite electrodes, one coated with a mixture of activated carbon powder and a polymer solution, which is called "capacitive" and the other unmodified, called "non-capacitive". The authors found that the bioanode that developed on the capacitive electrode was able to recover 52.9 % more charge than the non-capacitive electrode. It has also been demonstrated that the inherent capacitance of bioanodes can be exploited to increase power density production in microbial fuel cells by alternating open and close circuit operation [22,23].

Much less attention has been paid to the energy storage capabilities of biocathodes. To the best of our knowledge, only the work of Gomez Vidales et al. [24] have addressed the study of capacitance of methanogenic biocathodes. In the referred study, the authors used electrochemical characterisation analyses to show a progressive increase in the internal capacitance of the whole cell from 2.4 F to 3.6 F, a result that suggest that biocathodes can be used not only for long-term energy storage (following a power-to-gas approach) but also for short-term energy storage (in the form of an electric field in the electrode) [24]. Moreover, capacitive biocathodes can also provide a more flexible operation of BES as the charge storage in the electrode can buffer discontinuities in the power supply, a feature of great relevance within the context of high penetration of renewable energies [25]. Therefore, this is a topic worth investigating and so in the present study we aim at gaining a deeper understanding of the charge storage capabilities of biocathodes by investigating the effect of the duration of the charge/discharge periods, the polarization potential during discharge, and the modification of the supporting electrode with graphene oxide.

2. Materials and methods

2.1. Reactors setup and operational conditions

Two pieces (7.0 cm × 3.0 cm × 0.5 cm each) of carbon felt (soft felt SIGRATHERM GDF-2, SGL Carbon Group, Wiesbaden, Germany) were used as working electrodes, and were pre-treated according to method described in [26]. One of them was modified with graphene oxide following the method described in Section 2.2, while the other remained unmodified. The charge storage capabilities were studied in abiotic conditions (uncultured electrodes) and in biotic conditions (cultured electrodes with biocatalytic activity). This resulted in 4 different types of electrodes, that will be referred to as:

AC_{GO}: Abiotic Cathode modified with Graphene Oxide.
AC_{UM}: Abiotic Cathode UnModified.
BC_{GO}: Biotic Cathode modified with Graphene Oxide.
BC_{UM}: Biotic Cathode UnModified.

The biotic electrodes were cultured independently using two double-chamber H-cell reactors that consisted of two identical 500 mL glass bottles (Adams & Chittenden, Scientific glass; USA) separated by a cation exchange membrane (Fig. 1). A platinum wire mesh (2 cm × 2 cm, Goodfellow, UK) was place in the anode and served as a counter electrode. An Ag/AgCl (3 M KCl) reference electrode (Sigma-Aldrich® glass reference electrode, glass 12 mm; Germany) was placed in the cathode chamber in the vicinity of the working electrodes. The reactors were kept inside a temperature-controlled chamber (Fitotron, SANYO) that maintained the temperature at 30 ± 0.5 °C and were stirred at 250 rpm (Magnetic stirrer plate IKA-WERKE RO 15, Germany) to prevent mass transfer limitations.

The biotic electrodes were inoculated with the effluent from the cathodic chamber of a CH_4-producing microbial electrosynthesis cell that has been operated in our laboratory for +200 days (80 % inoculum and 20 % culture medium, adjusting to pH 7), and were polarized at −1.0 V vs. Ag/AgCl (3 M KCl) using a multichannel Biologic VSP potentiostat (Seyssinet-Pariset, France) equipped with an EC-Lab software (vs. 11.36) to promote the development of electroactive cathodophilic communities. The activation of the electrodes was carried out in batch mode with a cycle duration of 4–5 days, and it took 15–17 cycles for the electrodes to produce fairly reproducible current profiles across cycles. The biocathodes were allowed an additional maturation period of 15 cycles before the electrochemical characterisation and the

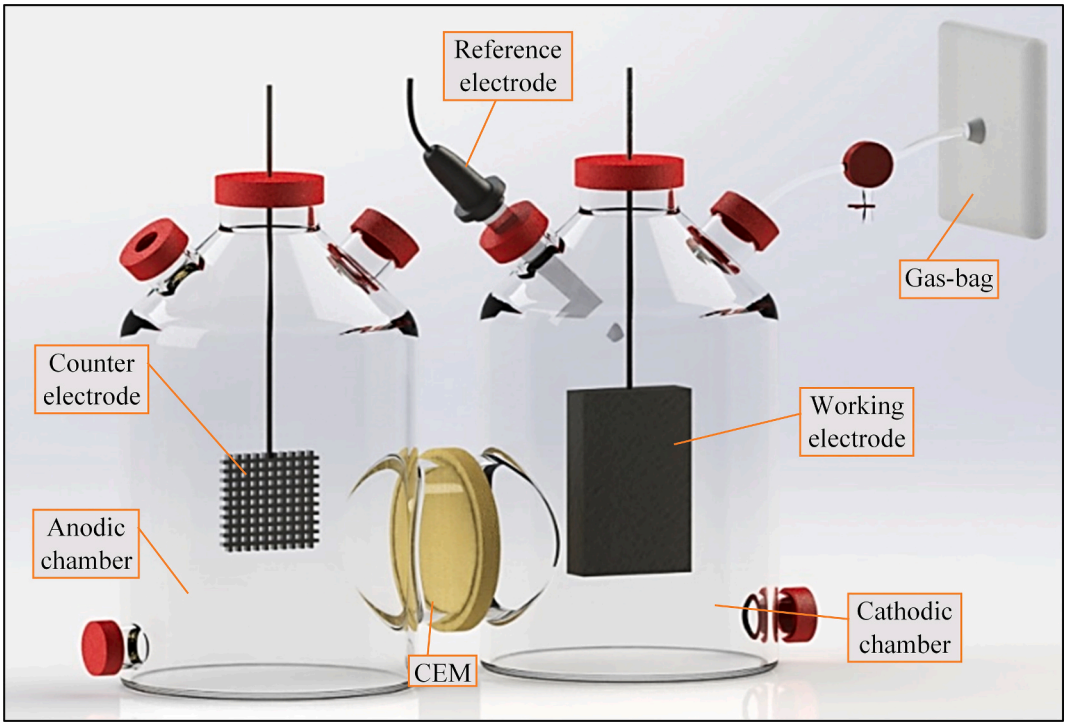

Fig. 1. Lab reactor configuration.

charge/discharge test begun. The catholyte (culture medium) consisted of 3.21 g K_2HPO_4, 1.57 g KH_2PO_4, 0.01 g $CaCl_2$, 0.09 g $MgCl_2$, 0.01 g $MgSO_4$ and 0.28 g NH_4Cl (pH 7.1); 1 mL of mineral solution and 1 mL of vitamin solution per litter [27]. The same medium was used for the anolyte, although without the vitamin solution to avoid the growth of microorganisms. Both the anolyte and catholyte were replaced with fresh medium at the beginning of each cycle. The catholyte was bubbled with nitrogen for 15 min to maintain anoxic conditions, and after closing the reactor, 350 mL of CO_2 gas were fed to the cathode chamber with the aid of a 1 L gas-bag (Ritter, Germany).

2.2. Graphene oxide electrodeposition and electrodes surface characterisation

AC_{GO} and BC_{GO} electrodes were modified by electrodeposition of graphene oxide (GO; 4 mg mL^{-1} dispersion in H_2O, SIGMA-ALDRICH Chemie GmbH, Germany). The electrodeposition was performed in an oxygen-free environment (nitrogen bubbling) using the Biologic VSP potentiostat and following the methodology described elsewhere [28]. The counter electrode was a platinum wire mesh (2 cm × 2 cm, Goodfellow, UK).

The microstructure of the abiotic electrodes was examined by means of JEOL JSM-6480LV scanning electron microscope (SEM) following the methodology reported in [28], to assess the correct electrodeposition on the carbon electrodes. The electrode surfaces were carefully cut, rinsed in deionised water, and dried at room temperature. Prior to SEM analysis, the specimens were sprayed with a thin layer of gold using a Leica EM ACE600 equipment.

2.3. Electrochemical characterisation and charge-discharge tests

The electrochemical performance of the electrodes was characterised by means of cyclic voltammetry (CV) and electrochemical impedance spectroscopy (EIS) techniques. CVs were conducted under no-turnover conditions at a scan rate of 5 $mV{\cdot}s^{-1}$ in a potential window between −1.2 V and 0 V. EIS analyses were carried out in a frequency range between 10^5 and 10^{-2} Hz and the electrode was polarized at the open circuit voltage.

The energy storage capabilities of the electrodes were also investigated by means of charge-discharge experiments at different cycles' duration as summarized in Table 1. The charging of the electrodes occurred in open circuit conditions, while the discharging took place at a fixed potential (−0.8, −1.0 and −1.2 V vs Ag/AgCl). The combination of the 5 charge-discharge cycles and 3 discharging potentials resulted in 15 different experimental conditions. In addition, each condition was maintained through ten consecutive cycles. Prior to every new experimental condition, the electrodes were fully discharge for one hour at a potential of −1.0 V. To clarify this, and by way of example, Fig. 3 represents the experimental sequence for test number 1 in Table 1.

2.4. Calculations

The total charge density (Q_t, $C{\cdot}m^{-2}$) was calculated by integrating the measured current density (ρ_i, $A{\cdot}m^{-2}$) —represented by the green line in Fig. 2b—, over the discharging time (Eq. (1)):

$$Q_t = \int_{t_1}^{t_2} \rho_i dt \tag{1}$$

where t_1 and t_2 are the initial and final discharging times in seconds.

Q_t is made of two components: the faradaic charge (Q_f, $C{\cdot}m^{-2}$), associated to (bio)-electrochemical reactions, and the capacitive charge (Q_c, $C{\cdot}m^{-2}$), that has to do with the (pseudo)-capacitive charge-storage phenomena. The current profiles of bioelectrodes typically display a sharp peak current upon reconnection that attenuates in time to a steady state current (Fig. 2b). Following [22], we assume that the steady state current corresponds to the faradaic component (ρ_f) of total current, and therefore Q_f can be calculated as:

$$Q_f = \rho_f (t_2 - t_1) \tag{2}$$

which corresponds to the blue shaded area in Fig. 2b. The orange shaded area Q_c, which can be assimilated to the capacitive charge released during the discharge period, can then be computed as:

$$Q_c = Q_t - Q_f \tag{3}$$

The charge storage efficiency (η_{Qc}) is a parameter used in this study to estimate the fraction of the total circulating charge that corresponds to capacitive charge. It is calculated according to the following expression:

$$\eta_{Qc} = \frac{Q_c}{Q_t} \tag{4}$$

Table 1
Charge-discharge timing selected for the different experiments.

Test nr.	Charging time (min)	Discharging time (min)
1	1	3
2	5	10
3	10	20
4	15	30
5	30	60

3. Results and discussion

The aim of this study is to explore the energy storage capabilities of carbon-felt-based methanogenic biocathodes under two circumstances, namely: with and without graphene oxide, by conducting charge-discharge experiments. Sections 3.1 and 3.2 will provide an electrochemical characterisation of the electrodes in abiotic and biotic conditions respectively, while Section 3.3 contains the results of the charge-discharge experiments, where we estimate the actual charge storage capabilities of the electrodes.

The graphene oxide electrodeposition was made through consecutives CV cycles (see Section 2.2), and the resulting CV profiles can be seen in the Supplementary information (Appendix A, Fig. A.1). SEM images at ×500 magnification (Fig. 3) confirm the electrodeposition and show that the graphene oxide treated cathode (AC_{GO}) is coated with an amorphous layer of graphene (Fig. 3b), that covers and extends between consecutive fibres, forming a discontinuous coating. Similar SEM images have been obtained in previous studies after the electrodeposition of carbon felt electrodes with graphene oxide [28–30].

3.1. Electrochemical characterisation of electrodes in abiotic conditions

Following the graphene oxide electrodeposition, the abiotic electrodes were electrochemically characterised by means of CV tests (Fig. 4a). Although neither of the abiotic electrodes (AC_{GO} and AC_{UM}) revealed significant electrochemical activity, the voltammogram of the AC_{GO} was wider than that of the AC_{UM}, which reveals a higher electrical capacitance. This could be linked to the higher roughness of the AC_{GO} electrode (as revealed by the SEM images in Fig. 3b) which results in a higher specific surface area [22] and therefore a higher double layer capacitance.

The electrochemical characterisation was complemented by EIS analyses (Fig. 4b). The resulting data were fitted to a modified Randle's equivalent electrical circuit (EEC) model (Fig. 4c) consisting of a an ohmic resistance (R_S), a charge transfer resistance (R_{CT}), a constant phase element (CPE) and an open Warburg element [31]. The corresponding model parameters for the abiotic electrodes are given in Table 2.

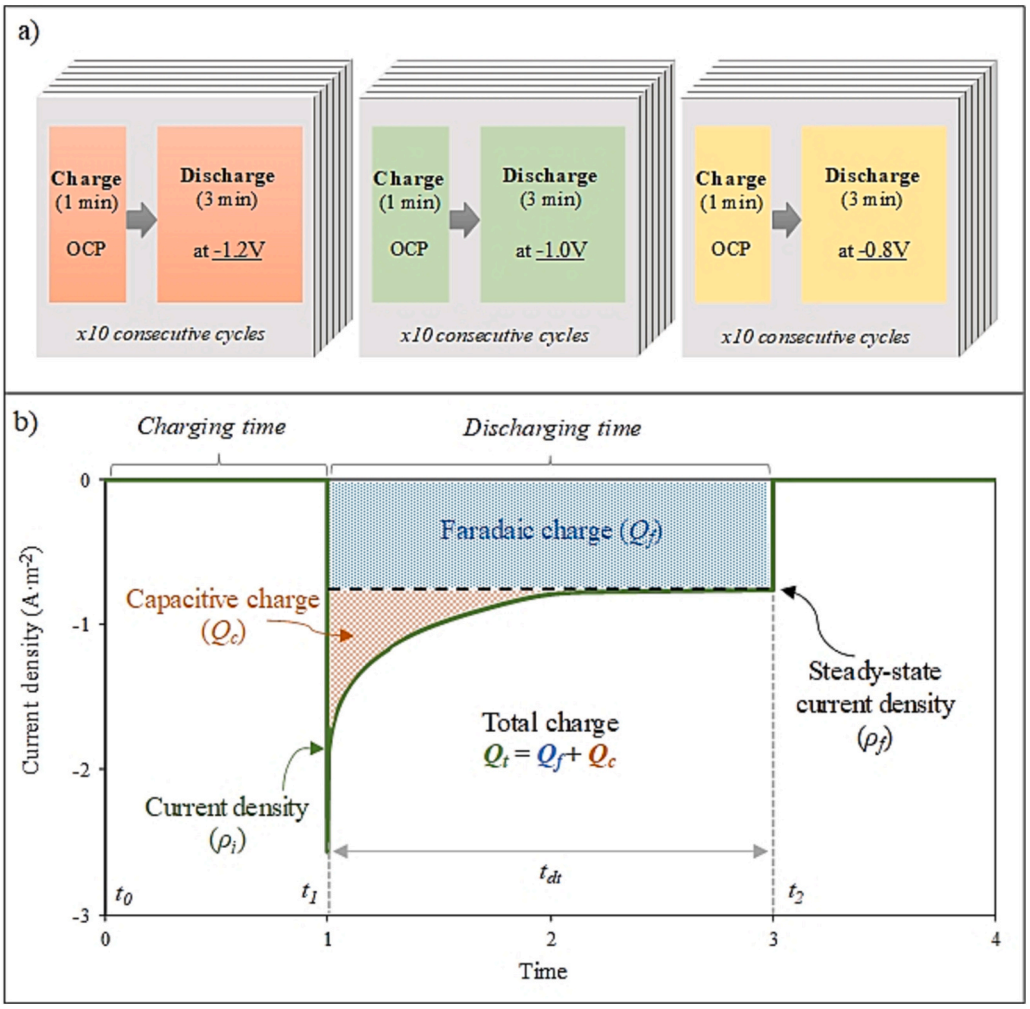

Fig. 2. a) Experimental sequence for test nr. 1 in Table 1, and b) Theoretical charge-discharge current profile. The total charge (Q_t) is made of two components: the faradaic charge (Q_f, blue shaded area) and the capacitive charge (Q_c, orange shaded area). (For interpretation of the references to colour in this figure legend, the reader is referred to the web version of this article.)

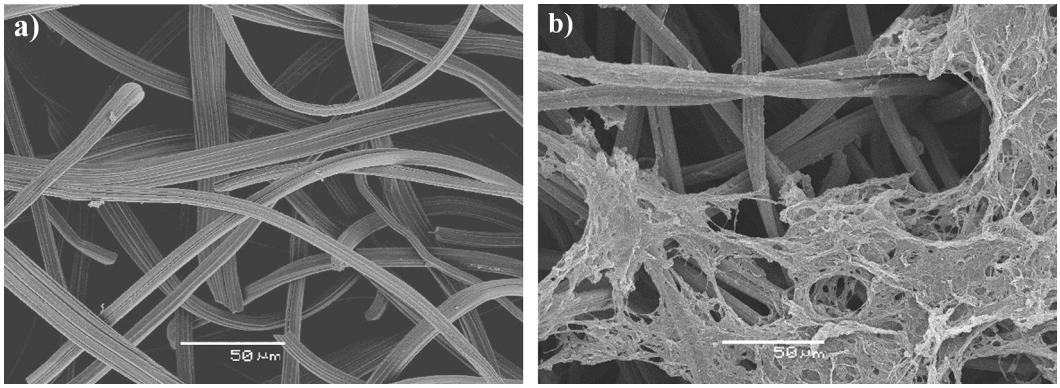

Fig. 3. SEM images of the abiotic electrodes before (left) and after (right) graphene oxide electrodeposition (×500 magnification).

Contrary to our expectations, the R_{CT} —that essentially represents the resistance of electron transfer between phases (e.g., electrode-electrolyte)— was almost 80 % lower in the AC_{UM} electrode compared to the AC_{GO}, indicating that the graphene oxide coating might be deteriorating the kinetics of the electron transfer for any abiotic background reaction. The CPE, which is related to double-layer capacitance in solid 3D electrodes [32], usually appears in the EEC of electrodes with fractal interface geometry [33] and/or defects that causes inhomogeneous current distribution [34,35]. It is defined by two parameters: Q and n. Parameter "n" adopts values between 0 and 1, and the higher it is the closer the CPE gets to an ideal capacitor. In addition, the double-layer capacitance of electrodes with CPE behaviour is proportional to the parameter Q [36], which in this study is almost 3 times larger in the AC_{GO} electrode, indicating that the graphene-treated electrode displays

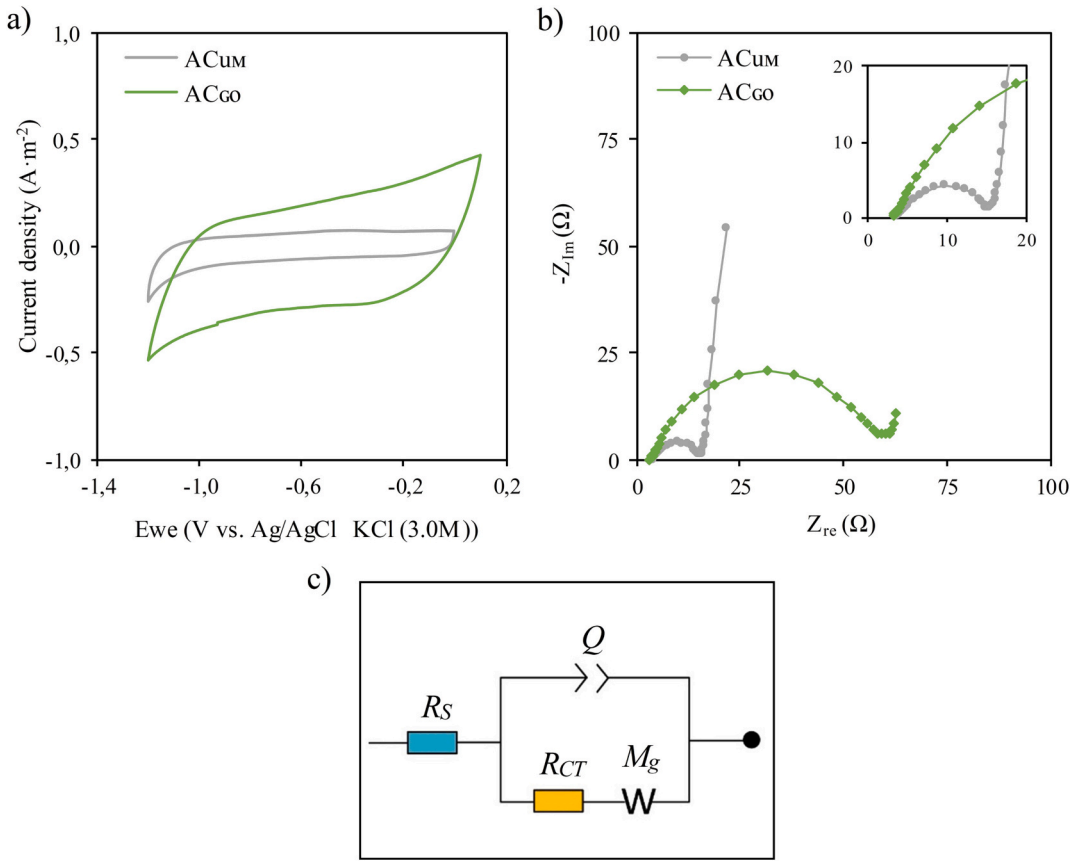

Fig. 4. Electrochemical characterisation of the abiotic electrodes: a) CV results, b) EIS results (Nyquist plot) and c) the equivalent electrical circuit used to fit the EIS data.

Table 2
EIS fitting data for the biotic electrodes: AC_{UM} and AC_{GO}.

Parameter	Units	AC_{UM}	AC_{GO}
R_S	Ω	4.1	3.5
R_{CT}	Ω	11.8	57.7
Q	$F{\cdot}s^{(n-1)}$	1.6E-4	3.9E-4
n	–	0.76	0.77

a larger capacitance compared to the unmodified one, something that is coherent with the CV results.

Parameter R_S, that models the total ohmic resistances —comprising the electrolyte, the electrode and the contact resistance between the electrode and the current collector [10]— was, as expected, similar in both electrodes as they were immersed in the same electrolyte and assembled in a similar way.

3.2. *Electrochemical characterisation of the biologically activated electrodes*

Following the abiotic characterisation, the electrodes were inoculated and polarized at −1.0 V to promote the formation of an electroactive biofilm [9,13]. The biocathode that resulted from the graphene-oxide electrodeposited electrode will be referred to as BC_{GO}, while the biocathode that developed on the bare carbon felt electrode will be named BC_{UM}.

Current started to grow on both electrodes after 2 cycles (approx. 10 days), and after 15 cycles the current profiles began to be repeatable (Fig. 5a shows the last 2 cycles), achieving a maximum peak current of -0.69 $A{\cdot}m^{-2}$ for BC_{UM} and -0.92 $A{\cdot}m^{-2}$ for BC_{GO}. In addition, the biocathodes were allowed 10 additional cycles to make sure that the microbial biofilms were mature enough before characterisation. As with the abiotic electrodes, the electrochemical performance of the bio-electrodes was assessed by means of CV and EIS tests (Fig. 5b and c respectively).

The most prominent feature of the biotic electrodes (compared to abiotic ones) was perhaps the appearance of a large catalytic wave clearly visible at potentials below −0.9 V, that can be attributed to the hydrogen evolution reaction [9,13]. The size of the peak was distinctively larger (absolute value) for the BC_{GO}, which indicates an enhanced biocatalytic activity, most probably due to the presence of the graphene-oxide coating. In addition, the voltammogram recorded on the BC_{GO} was wider than that on the BC_{UM}, which is indicative of a larger capacitance. These results corroborate the beneficial impact of graphene on the performance of bioelectrodes (for both bioanodes [28,37,38], and biocathodes [13,39,40]).

The EEC that resulted from the EIS analyses was similar to that obtained for the abiotic electrodes, although it required additional elements to suitably fit EIS data (Fig. 5d): in addition to R_S, R_{CT}, CPE and W (originally present in the abiotic EEC), the biotic circuits incorporated two additional elements: a resistance (R_{BIO}) and a capacitance (C_{BIO}), that can be attributed to the ohmic resistance and capacitance of the electroactive biofilm [18]. The fitted parameters of the EEC for the biotic electrodes are collected in Table 3.

In contrast to the results obtained for the abiotic electrodes, where graphene electrodeposition negatively affected the charge transfer resistance, the biocathode that contained graphene (BC_{GO}) presented a much lower charge transfer resistance (R_{CT} in Table 3) compared to BC_{UM}. This indicates that graphene favoured the exchange of electrons between the electrode and the biofilm, which is coherent with the larger catalytic wave obtained for the BC_{GO} (Fig. 5b). In addition, the ohmic resistance of the biofilm (R_{BIO} in Table 3), and the two parameters

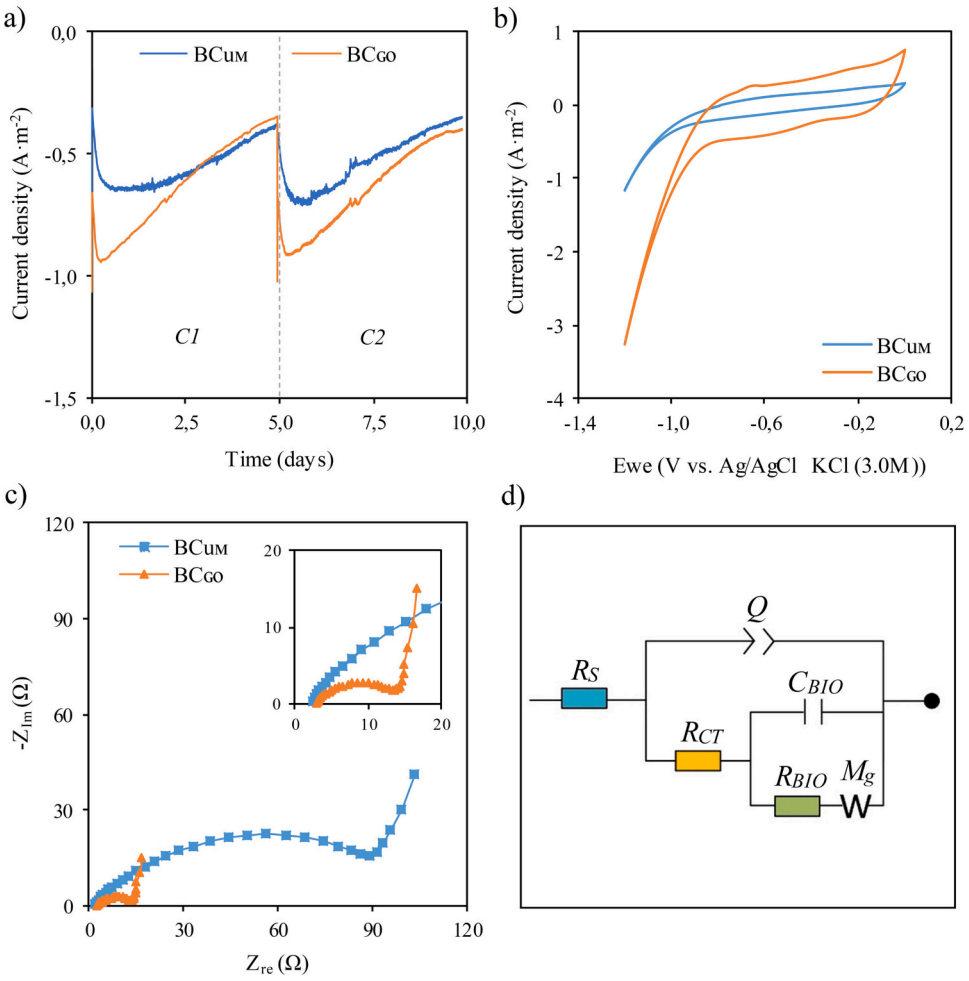

Fig. 5. Characterisation of the biotic electrodes: a) current profiles recorded during the last 2 cycles of the start-up period; b) CV results; c) EIS results (Nyquist plot); and d) equivalent electrical circuit used to fit EIS results.

Table 3
EIS fitting data for the biotic electrodes: BC_{UM} and BC_{GO}.

Parameter	Units	BC_{UM}	BC_{GO}
R_S	Ω	1.3	2.5
R_{CT}	Ω	106.1	13.27
Q	$F{\cdot}s^{(n-1)}$	1.1E-3	3.7E-03
n	–	0.50	0.48
R_{Bio}	Ω	255.4	107.7
C_{Bio}	mF	38.6	93.4

related to charge storage (CPE and C_{BIO}) were around three times more favourable in the BC_{GO} electrode. This again can be attributed to the graphene coating that, as observed in other studies, increases the robustness of the electrode and allows a better grip and growth of the electroactive biofilm [22,29,30].

3.3. Charge-discharge experiments

The results presented in the previous sections suggest superior energy storage capabilities of the graphene treated electrodes (both in abiotic and biotic conditions). To confirm these results and to provide a more explicit quantification of the charge storage capacities, the biotic and abiotic electrodes were subjected to a set charge-discharge experiments. In these experiments, charging periods (open circuit conditions) were alternated with discharging periods at three different poised potentials: −1.2 V, −1.0 V and −0.8 V. In addition, and to investigate whether the duration of cycling has any influence on the stability of the electrodes, the length of charging and the discharging intervals was varied. Fig. 6 presents, by way of example, the potential and current density profiles for a charging time of 10 min and discharging time of 20 min. The whole series of current and potential profiles for all the electrodes and cycling durations can be consulted in the Supplementary material (Appendix A, Figs. A.2 & A.3).

The potential profiles of the abiotic electrodes obtained during the charging period differed significantly from those of the biotic electrodes (Fig. 6a). In the former (green and grey lines in Fig. 6a), the potential increases steadily throughout the charging, and does not seem to converge to any stable potential. This was especially visible for the AC_{UM} electrode, in which the potential increased more rapidly, achieving higher final potentials. Contrastingly, the potential in the AC_{GO} electrode grew at a lower rate, which is indicative of a larger time constant, being consistent with the larger capacitance and the larger charge transfer resistance measured for this electrode (Table 2).

Unlike the abiotic electrodes, the potential profiles of the biotic electrodes (orange and blue lines in Fig. 6a) were fairly similar between them, regardless of the presence of graphene. The biotic potential profiles showed two distinctive sections that were apparently absent in the abiotic ones: initially, and just after disconnection, potential raised almost immediately, evolving more gradually in the following seconds, and converging to a final potential of about −0.73 V. This behaviour suggests the existence of two different time constants, something that would be coherent with the existence of two energy storage elements in the equivalent electric circuit (CPE and C_{BIO}).

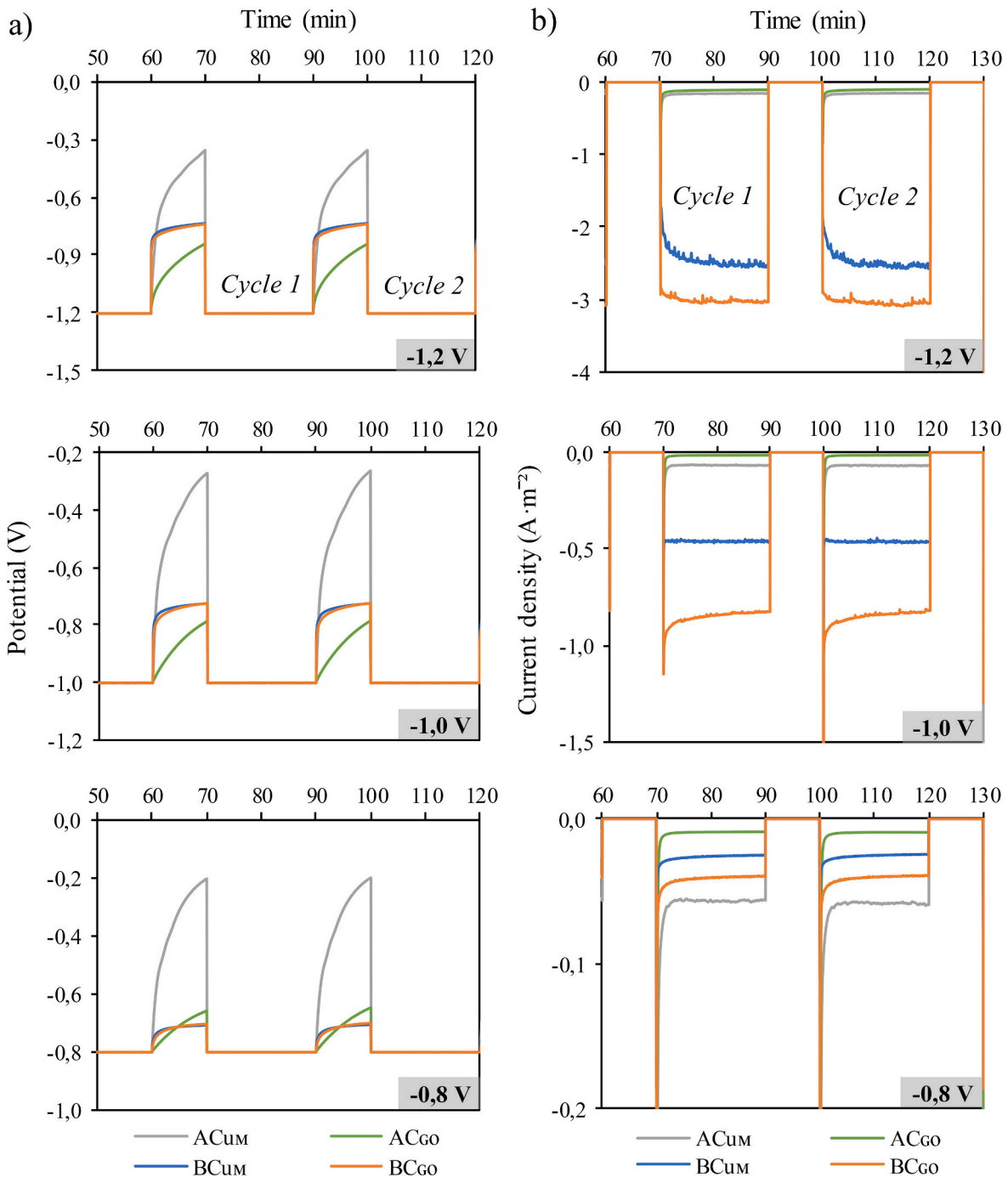

Fig. 6. a) Potential profiles and b) current density profiles for 2 cycles of 10 min charging and 20 min discharging experiment. (For interpretation of the references to colour in this figure, the reader is referred to the web version of this article.)

Although the total charge stored during the charging period cannot be directly measured (because it is not possible to measure current), it can be roughly estimated through the expression $C \times (V_f - V_i)$, which corresponds to the charge stored in an ideal capacitor when potential evolves from V_i (initial potential) to V_f (final potential). The parameter "C", that represents the capacitance (in Farads) of biotic electrodes, can be directly obtained from Table 3. In addition, and as mentioned above, the CPE also contributes to the overall double-layer capacitance of both biotic and abiotic electrodes [36]. This contribution can be estimated from the parameter "Q" (Tables 2 and 3), as the double layer capacitance of an electrode with CPE behaviour is proportional to Q [36]. However, the values of V_i and V_f cannot be directly measured for the individual elements of the EEC. Nevertheless, if we assume that the electrical potential in these elements evolves following a trend similar to that of the electrode potential (Fig. 6a), then it is possible to have a rough (qualitative) estimate of the potential step they underwent. Thus, for the biotic electrodes, we can say that the BC_{GO} is storing more charge that BC_{UM} because the difference between V_i and V_f is slightly higher, and because the value of C in the two elements capable of storing charge (C_{BIO} and CPE) is about 3 times larger. For the abiotic electrodes we find a more complex situation, as the electrode with the larger capacitance (AC_{GO}) undergoes the smaller potential change (and vice versa) and therefore it is not possible to provide a straightforward estimate as with the biotic electrodes.

The current released during the discharge periods (Fig. 6b) can potentially provide a better (quantitative) estimate of the charge stored (Q_c), although this alternative also has its own limitations. This is because the measured current is made up of two components: the faradaic current —that involves (bio)-electrochemical reactions— and the capacitive (non-faradaic) current, that is related to charge storage phenomena. The latter, in turn, also has two components: a purely capacitive current connected to electrostatic processes (double-layer phenomena) and a pseudocapacitive current, produced by quick faradaic reactions [41], that in biological electrodes involves fast redox reactions of the bacterial cytochromes present in electroactive biofilms [42]. Although it is no easy to discriminate between the different contributions [22], we have followed the method described in [22] to have an estimate of the charge stored/released. In the referred work it is assumed that the discharge of the electrodes is usually accompanied by a sharp peak of current (just upon reconnection) that attenuates in time towards a steady (or pseudo-steady) state current. By assuming that the steady state current corresponds to the faradaic current, we can approximate the amount of charge stored/released (that lumps together the capacitive and pseudocapacitive components) by subtracting the steady state-faradaic charge Q_f from the total measured charge Q_t following Eq. (4) (for more details, see Section 2.3 in M&M).

As expected, Q_t in any of the electrodes increased with the duration of the discharging period (Fig. 7), with the biotic electrodes always producing more charge at −1.0 V and −1.2 V. However, when the potential was set at −0.8 V, current production collapsed, and the abiotic electrodes showed a comparable and even superior performance. It seems that at −0.8 V the electrotrophic activity becomes severely limited, and the biofilm acts as a barrier to any background current. It is also interesting to note that although graphene-oxide electrodeposition enhanced the performance of the biotic electrodes —a result reported in other studies [13,30,43]—, it hindered the production of faradic background current, which is consistent with lower charge transfer resistance for the AC_{UM} (Table 2). This might be caused by the discontinuous graphene oxide coating visible in the SEM images (Fig. 3b), that might be blocking the entry of the electrolyte inside the electrode.

The peaks associated to the release of (pseudo)-capacitive charge were always clearly visible in the abiotic electrodes. However, they apparently disappeared from the biotic ones for some charge-discharge periods at a discharging potential of −1.2 V (Appendix A, Fig. A.3). For example, for a 10 min charging and 20 min discharging periods at −1.2 V (Fig. 6b), neither the BC_{UM} nor the BC_{GO} showed this peak. This can probably be attributed to the fact that the biocathodes were cultured at −1.0 V, so polarizing them at a more reducing potential might be producing an in-rush of faradaic current that masks any charge-release peak (the steady state faradaic current at −1.2 V was about 3–4 times larger

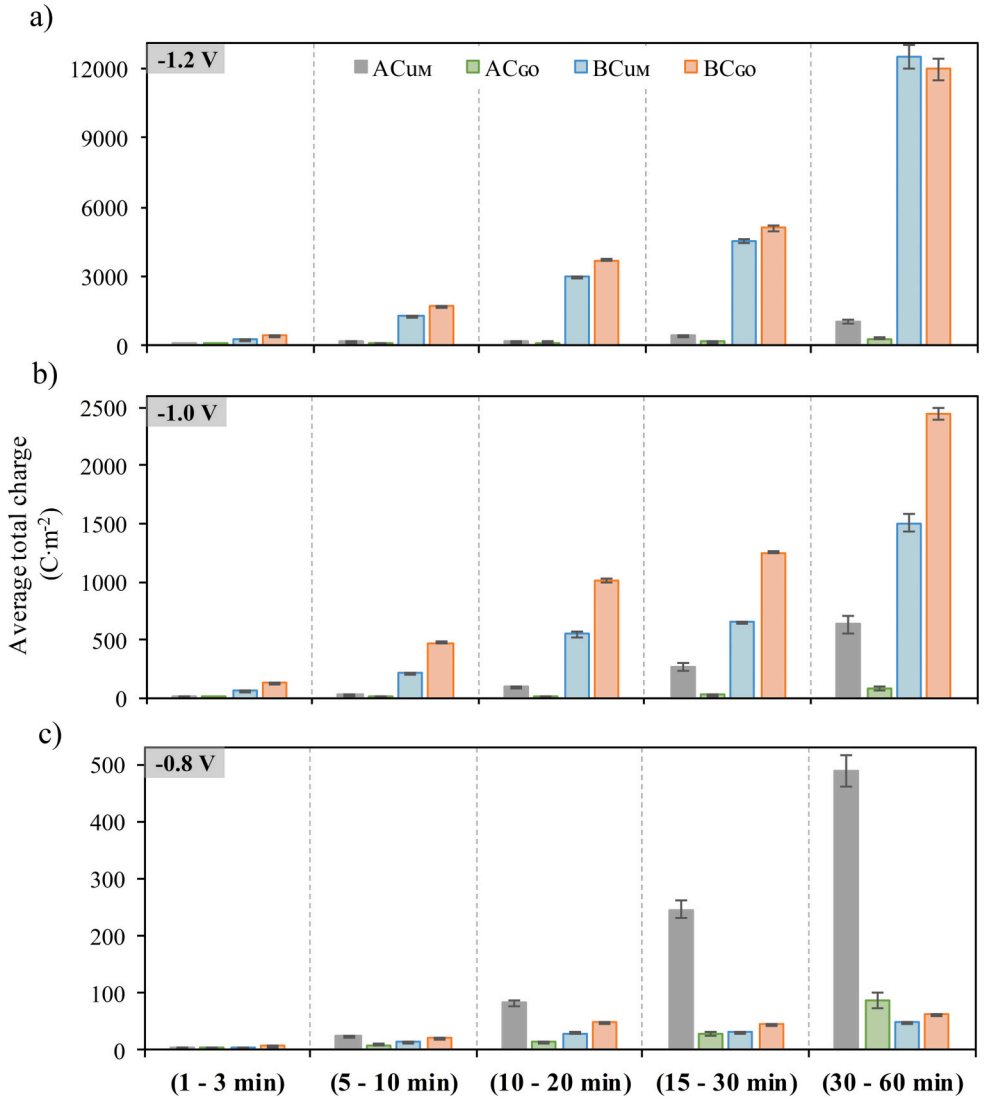

Fig. 7. Average total charge (Q_t) of the electrodes at different charge-discharge times at: a) −1.2 V; b) −1.0 V; and c) −0.8 V.

than that at −1.0 V). Moreover, the current profiles at −1.2 V were highly inconsistent across the different cycling periods (see Fig. A.3, Appendix A), also showing a significant amount of noise (especially in the BC_{UM}), that might be related to unstable bioelectrochemical reactions at large polarization potentials.

In contrast, when the discharging potential was set at −1.0 V, the peaks associated to the release of stored charge became always clearly visible for the BC_{GO}, and the amount of (pseudo)-capacitive charge they produced was far superior to any of the other electrodes. In addition, the current density evolved more gradually in them (Fig. A.3), revealing a larger time constant which again is indicative of a larger storage capacity, something that is coherent with results presented in Table 3.

For the BC_{UM}, the peaks at −1.0 V were so thin that the amount of (pseudo-)capacitive charge they released was almost negligible, even falling below the capacitive current measured for the abiotic electrodes. When the discharge potential was set at −0.8 V, the peaks became clearly discernible for all the electrodes. However, the amount of (pseudo)-capacitive charge produced by the biotic electrodes was always inferior to that of the abiotic ones. As mentioned above, it seems that the electroactivity of the biofilm at −0.8 V not only gets greatly diminished, but it creates a barrier that hampers performance. This result might be indicating that only a small fraction of the charge stored/released in the BC_{GO} at −1.0 V and −1.2 V is related to double-layer (capacitive) phenomena, while most of it (between 94 and 98 %) is of pseudo-capacitive origin (i.e.: current related to the metabolic activity of the electroactive biofilm and not to double-layer phenomena).

Results also indicate that, contrary to expectations, the AC_{UM} electrodes are capable of storing more charge than the AC_{GO} (Fig. 8a), which is in apparent contradiction with the EIS results presented in Fig. 4b, where the AC_{GO} electrode scored a larger capacitance (as estimated from the CPE). However, as the total charge stored depends not only on capacitance but also on the difference between initial and final electrode potential (which is higher for the AC_{UM}, Fig. 6a), it can be hypothesized that the contribution of the potential step to charge storage is more determinant than the capacitance of the electrode.

Finally, the charge storage capabilities of the electrodes were characterised in terms of charge storage efficiency (η_{Qc}), which compares the (pseudo)-capacitive current Q_c against the total circulating current Q_t for a particular charge/discharge cycle (using Eq. (4)). Results indicate that η_{Qc} was almost always far superior for the abiotic electrodes, reaching a maximum for a charging period of 5 min (Fig. 8b). In addition, and despite its lower capacitance, the AC_{GO} electrode always showed the

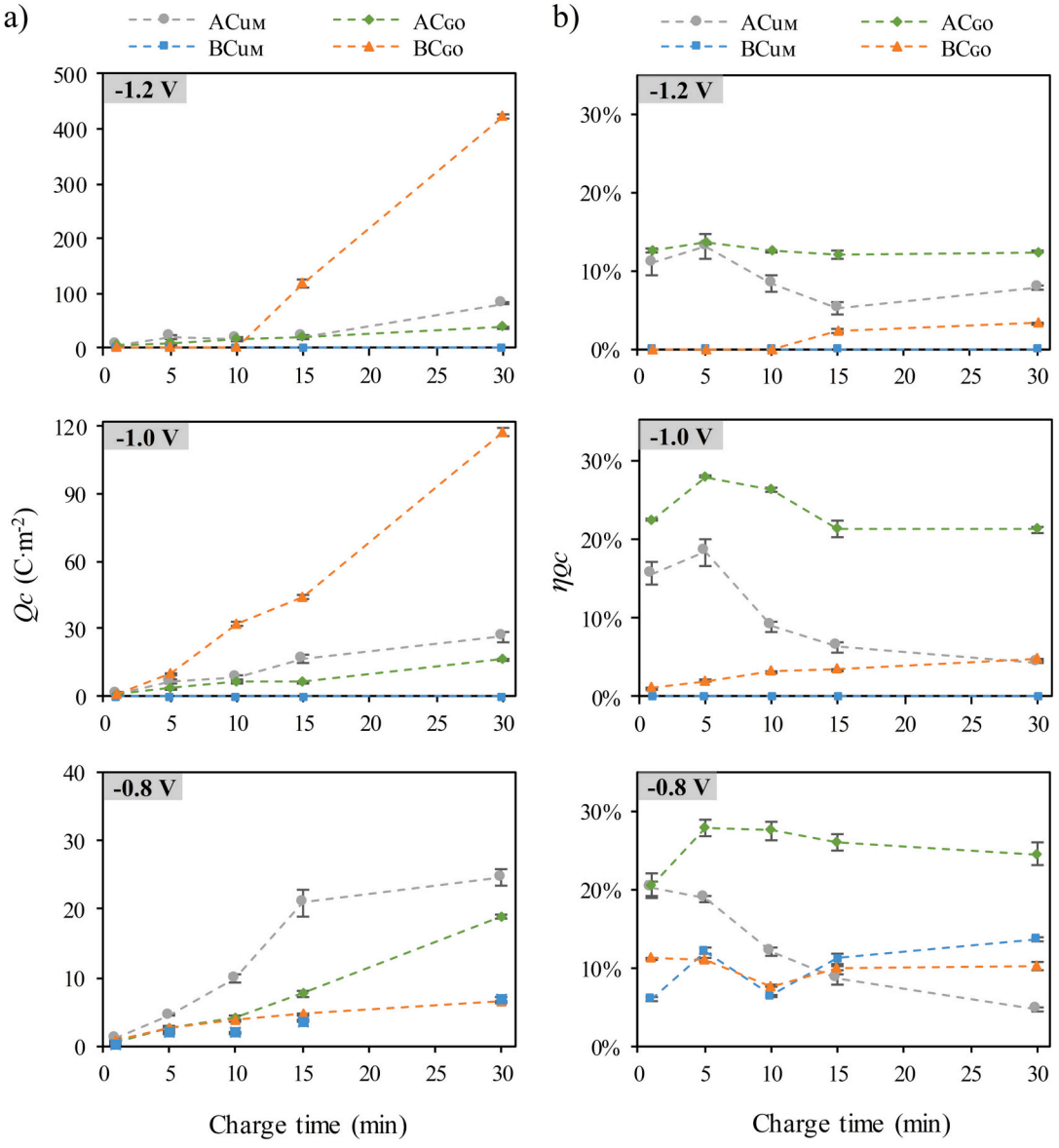

Fig. 8. a) Charge storage (Q_c), and b) recovery coefficient (η_{Qc}) at different potential and charging times.

best performance regardless of the cycling duration and the discharging potential, achieving η_{Qc} of up to 30 %. This can be possibly attributed to the lower background current compared to the AC_{UM}. In contrast, the η_{Qc} of the biotic electrodes was always below 5 % at discharging voltages of −1.0 V and −1.2 V, with the BC_{GO}.

4. Conclusions

In this study we explore the charge storage capabilities of methane-producing biocathodes under two circumstances: with and without graphene oxide electrodeposition. Results seem to indicate that although the graphene electrodeposition has a positive effect in the electrochemical performance of the biotic electrodes, it deteriorates both the kinetics and the charge storage capabilities of the abiotic ones. It is also important to note that the energy storage capabilities of biotic electrode without graphene were greatly diminished, to such an extent, that even the abiotic electrodes showed a greater capacity in all the experimental conditions. For the graphene-treated electrode, the discharging potential had a definite impact not only on current production but also on charge storage capacity: large potentials induced an inrush of faradaic current that in many cases masked any peak associated to the release of capacitive charge. These peaks became clearly visible at low potentials, although the charge stored in them was lower than that of abiotic electrodes. Finally, results indicated that more than 90 % of the charge stored in the biotic electrode treated with graphene was due to pseudo-capacitive phenomena (i.e.: fast redox reactions).

CRediT authorship contribution statement

D. Carrillo-Peña: Conceptualization, Investigation, Methodology, Writing – original draft. **G. Pelaz:** Investigation. **R. Mateos:** Supervision, Investigation, Methodology. **A. Escapa:** Conceptualization, Supervision, Methodology, Writing – review & editing, Funding acquisition, Project administration.

Declaration of competing interest

The authors declare that they have no known competing financial interests or personal relationships that could have appeared to influence the work reported in this paper.

Data availability

Data will be made available on request.

Acknowledgments

This research was possible thanks to the financial support of “Ministerio de Ciencia e Innovación” project ref: TED2021-129687A-I00, financed by MCIN/AEI/10.13039/501100011033 and European Union NextGenerationEU/PRTR.

Appendix A. Supplementary data

Supplementary data to this article can be found online at https://doi.org/10.1016/j.est.2023.109789.

References

[1] Red Eléctrica Española, REData - Potencia instalada en España. https://www.ree.es/es/datos/generacion/potencia-instalada, 2023 (accessed June 7, 2023).
[2] J. Shair, H. Li, J. Hu, X. Xie, Power system stability issues, classifications and research prospects in the context of high-penetration of renewables and power electronics, Renew. Sust. Energ. Rev. 145 (2021), 111111, https://doi.org/10.1016/j.rser.2021.111111.
[3] X. Li, M. Paster, J. Stubbins, The dynamics of electricity grid operation with increasing renewables and the path toward maximum renewable deployment, Renew. Sust. Energ. Rev. 47 (2015) 1007–1015, https://doi.org/10.1016/J.RSER.2015.03.039.
[4] C. Yagi, K. Takeuchi, Estimating the value of energy storage: the role of pumped hydropower in the electricity supply network, Japan World Econ. 68 (2023), 101210, https://doi.org/10.1016/J.JAPWOR.2023.101210.
[5] O. Fajinmi, J.L. Munda, Y. Hamam, O. Popoola, Compressed air energy storage as a battery energy storage system for various application domains: a review, Energies 16 (2023) 6653, https://doi.org/10.3390/EN16186653.
[6] K. Chandrasekhar, A.N. Kumar, T. Raj, G. Kumar, S.H. Kim, Bioelectrochemical system-mediated waste valorization, Syst. Microbiol. Biomanuf. 1 (2021) 432–443, https://doi.org/10.1007/S43393-021-00039-7.
[7] R. Blasco-Gómez, P. Batlle-Vilanova, M. Villano, M.D. Balaguer, J. Colprim, S. Puig, On the edge of research and technological application: a critical review of electromethanogenesis, Int. J. Mol. Sci. 18 (2017) 874, https://doi.org/10.3390/ijms18040874.
[8] F. Geppert, D. Liu, M. van Eerten-Jansen, E. Weidner, C. Buisman, A. ter Heijne, Bioelectrochemical power-to-gas: state of the art and future perspectives, Trends Biotechnol. 34 (2016) 879–894, https://doi.org/10.1016/j.tibtech.2016.08.010.
[9] G. Pelaz, D. Carrillo-Peña, A. Morán, A. Escapa, Electromethanogenesis at medium-low temperatures: impact on performance and sources of variability, Fuel. 310 (2022), 122336, https://doi.org/10.1016/J.FUEL.2021.122336.
[10] H.Y. Yang, B.L. Bao, J. Liu, Y. Qin, Y.R. Wang, K.Z. Su, J.C. Han, Y. Mu, Temperature dependence of bioelectrochemical CO2 conversion and methane production with a mixed-culture biocathode, Bioelectrochemistry 119 (2018) 180–188, https://doi.org/10.1016/j.bioelechem.2017.10.002.
[11] M. Hara, Y. Onaka, H. Kobayashi, Q. Fu, H. Kawaguchi, J. Vilcaez, K. Sato, Mechanism of electromethanogenic reduction of CO2 by a thermophilic methanogen, Energy Procedia 37 (2013) 7021–7028, https://doi.org/10.1016/j.egypro.2013.06.637.
[12] B. Bian, S. Bajracharya, J. Xu, D. Pant, P.E. Saikaly, Microbial electrosynthesis from CO2: challenges, opportunities and perspectives in the context of circular bioeconomy, Bioresour. Technol. 302 (2020), 122863, https://doi.org/10.1016/J.BIORTECH.2020.122863.
[13] D. Carrillo-Peña, R. Mateos, A. Morán, A. Escapa, Reduced graphene oxide improves the performance of a methanogenic biocathode, Fuel 321 (2022), 123957, https://doi.org/10.1016/j.fuel.2022.123957.
[14] G. Zhen, S. Zheng, X. Lu, X. Zhu, J. Mei, T. Kobayashi, K. Xu, Y.Y. Li, Y. Zhao, A comprehensive comparison of five different carbon-based cathode materials in CO2 electromethanogenesis: long-term performance, cell-electrode contact behaviors and extracellular electron transfer pathways, Bioresour. Technol. 266 (2018) 382–388, https://doi.org/10.1016/J.BIORTECH.2018.06.101.
[15] G. Pelaz, R. González, A. Morán, A. Escapa, Elucidating the impact of power interruptions on microbial electromethanogenesis, Appl. Energy 331 (2023), 120382, https://doi.org/10.1016/J.APENERGY.2022.120382.
[16] M. Shahparasti, S. Bouchakour, A. Luna, D. Molognoni, P. Bosch-Jimenez, E. Borràs, Simplified modelling of nonlinear electromethanogenesis stack for power-to-gas applications, J. Energy Storage 31 (2020), 101633, https://doi.org/10.1016/J.EST.2020.101633.
[17] K.R. Fradler, J.R. Kim, H.C. Boghani, R.M. Dinsdale, A.J. Guwy, G.C. Premier, The effect of internal capacitance on power quality and energy efficiency in a tubular microbial fuel cell, Process Biochem. 49 (2014) 973–980, https://doi.org/10.1016/J.PROCBIO.2014.02.021.
[18] A. Ter Heijne, D. Liu, M. Sulonen, T. Sleutels, F. Fabregat-Santiago, Quantification of bio-anode capacitance in bioelectrochemical systems using electrochemical impedance spectroscopy, J. Power Sources 400 (2018) 533–538, https://doi.org/10.1016/J.JPOWSOUR.2018.08.003.
[19] C. Santoro, F. Soavi, A. Serov, C. Arbizzani, P. Atanassov, Self-powered supercapacitive microbial fuel cell: the ultimate way of boosting and harvesting power, Biosens. Bioelectron. 78 (2016) 229–235, https://doi.org/10.1016/J.BIOS.2015.11.026.
[20] I. Ieropoulos, J. Greenman, C. Melhuish, J. Hart, Energy accumulation and improved performance in microbial fuel cells, J. Power Sources 145 (2005) 253–256, https://doi.org/10.1016/J.JPOWSOUR.2004.11.070.
[21] N. Uría, X. Muñoz Berbel, O. Sánchez, F.X. Muñoz, J. Mas, Transient storage of electrical charge in biofilms of Shewanella oneidensis MR-1 growing in a microbial fuel cell, Environ. Sci. Technol. 45 (2011) 10250–10256, https://doi.org/10.1021/ES2025214.
[22] A. Deeke, T.H.J.A. Sleutels, H.V.M. Hamelers, C.J.N. Buisman, Capacitive bioanodes enable renewable energy storage in microbial fuel cells, Environ. Sci. Technol. 46 (2012) 3554–3560, https://doi.org/10.1021/es204126r.
[23] X.A. Walter, J. Greenman, I.A. Ieropoulos, Intermittent load implementation in microbial fuel cells improves power performance, Bioresour. Technol. 172 (2014) 365–372, https://doi.org/10.1016/J.BIORTECH.2014.09.034.
[24] A. Gomez Vidales, S. Omanovic, B. Tartakovsky, Combined energy storage and methane bioelectrosynthesis from carbon dioxide in a microbial electrosynthesis system, Bioresour. Technol. Rep. 8 (2019), 100302, https://doi.org/10.1016/j.biteb.2019.100302.
[25] L. Caizán-Juanarena, C. Borsje, T. Sleutels, D. Yntema, C. Santoro, I. Ieropoulos, F. Soavi, A. ter Heijne, Combination of bioelectrochemical systems and electrochemical capacitors: principles, analysis and opportunities, Biotechnol. Adv. 39 (2020), 107456, https://doi.org/10.1016/J.BIOTECHADV.2019.107456.
[26] R. Mateos, R.M. Alonso, A. Escapa, A. Morán, Methodology for fast and facile characterisation of carbon-based electrodes focused on bioelectrochemical systems development and scale up, Materials 10 (2017) 79, https://doi.org/10.3390/ma10010079.

[27] M.C.A.A. van Eerten-Jansen, A.B. Veldhoen, C.M. Plugge, A.J.M. Stams, C.J. N. Buisman, A. ter Heijne, Microbial community analysis of a methane-producing biocathode in a bioelectrochemical system, Archaea 2013 (2013), 481784, https://doi.org/10.1155/2013/481784.
[28] R.M. Alonso, M.I. San-Martín, A. Sotres, A. Escapa, Graphene oxide electrodeposited electrode enhances start-up and selective enrichment of exoelectrogens in bioelectrochemical systems, Sci. Rep. 7 (2017) 13726, https://doi.org/10.1038/s41598-017-14200-7.
[29] Q. Fu, Y. He, Z. Li, J. Li, L. Zhang, X. Zhu, Q. Liao, Direct CO2 delivery with hollow stainless steel/graphene foam electrode for enhanced methane production in microbial electrosynthesis, Energy Convers. Manag. 268 (2022), 116018, https://doi.org/10.1016/J.ENCONMAN.2022.116018.
[30] N. Hu, L. Wang, M.G. Liao, K. Liu, Research on electrocatalytic reduction of CO2 by microorganisms with a graphene modified carbon felt, Int. J. Hydrog. Energy 46 (2021) 6180–6187, https://doi.org/10.1016/J.IJHYDENE.2020.11.127.
[31] N. Bonanos, B.C.H. Steele, E.P. Butler, J.R. Macdonald, W.B. Johnson, W. L. Worrell, A. Goossens, D.D. Macdonald, M.C.H. McKubre, E. Barsoukov, B. E. Conway, N. Wagner, Applications of impedance spectroscopy, in: Impedance Spectroscopy: Theory, Experiment, and Applications, Second edition, John Wiley & Sons, Inc., 2005, pp. 205–537, https://doi.org/10.1002/0471716243.CH4.
[32] A. Lasia, The origin of the constant phase element, J. Phys. Chem. Lett. 13 (2022) 580–589, https://doi.org/10.1021/ACS.JPCLETT.1C03782.
[33] I.D. Raistrick, D.R. Franceschetti, J.R. Macdonald, Theory, in: Impedance Spectroscopy: Theory, Experiment, and Applications, Second edition, John Wiley & Sons, Inc., 2005, pp. 27–128, https://doi.org/10.1002/0471716243.CH2.
[34] A. Gomez Vidales, S. Omanovic, H. Li, S. Hrapovic, B. Tartakovsky, Evaluation of biocathode materials for microbial electrosynthesis of methane and acetate, Bioelectrochemistry 148 (2022), 108246, https://doi.org/10.1016/J.BIOELECHEM.2022.108246.
[35] A. Sotniczuk, D. Kuczyńska-Zemła, A. Królikowski, H. Garbacz, Enhancement of the corrosion resistance and mechanical properties of nanocrystalline titanium by low-temperature annealing, Corros. Sci. 147 (2019) 342–349, https://doi.org/10.1016/J.CORSCI.2018.11.016.
[36] G.J. Brug, A.L.G. van den Eeden, M. Sluyters-Rehbach, J.H. Sluyters, The analysis of electrode impedances complicated by the presence of a constant phase element, J. Electroanal. Chem. Interfacial Electrochem. 176 (1984) 275–295, https://doi.org/10.1016/S0022-0728(84)80324-1.
[37] E. Roubaud, R. Lacroix, S. Da Silva, J. Esvan, L. Etcheverry, A. Bergel, R. Basséguy, B. Erable, Industrially scalable surface treatments to enhance the current density output from graphite bioanodes fuelled by real domestic wastewater, IScience 24 (2021), 102162, https://doi.org/10.1016/j.isci.2021.102162.
[38] E.T. Sayed, H. Alawadhi, A.G. Olabi, A. Jamal, M.S. Almahdi, J. Khalid, M. A. Abdelkareem, Electrophoretic deposition of graphene oxide on carbon brush as bioanode for microbial fuel cell operated with real wastewater, Int. J. Hydrog. Energy 46 (2021) 5975–5983, https://doi.org/10.1016/j.ijhydene.2020.10.043.
[39] J. Hu, C. Zeng, G. Liu, Y. Lu, R. Zhang, H. Luo, Enhanced sulfate reduction accompanied with electrically-conductive pili production in graphene oxide modified biocathodes, Bioresour. Technol. 282 (2019) 425–432, https://doi.org/10.1016/j.biortech.2019.03.023.
[40] J. Chen, Y. Hu, W. Huang, L. Zhang, Enhanced electricity generation for biocathode microbial fuel cell by in situ microbial-induced reduction of graphene oxide and polarity reversion, Int. J. Hydrog. Energy 42 (2017) 12574–12582, https://doi.org/10.1016/J.IJHYDENE.2017.03.012.
[41] F. Béguin, V. Presser, A. Balducci, E.F. Frackowiak Béguin, E. Frackowiak, V. Presser, A. Balducci, Carbons and electrolytes for advanced supercapacitors, Adv. Mater. 26 (2014) 2219–2251, https://doi.org/10.1002/ADMA.201304137.
[42] N.S. Malvankar, T. Mester, M.T. Tuominen, D.R. Lovley, Supercapacitors based on c-type cytochromes using conductive nanostructured networks of living bacteria, ChemPhysChem 13 (2012) 463–468, https://doi.org/10.1002/CPHC.201100865.
[43] M. Su, L. Wei, Z. Qiu, Q. Jia, J. Shen, A graphene modified biocathode for enhancing hydrogen production, RSC Adv. 5 (2015) 32609–32614, https://doi.org/10.1039/C5RA02695D.